Biochemical Pharmacology 82 (2011) 1549–1561

Contents lists available at ScienceDirect

Biochemical Pharmacology

journal homepage: www.elsevier.com/locate/biochempharm

Biochemical disorders associated with antiproliferative effect of dehydroepiandrosterone in hepatoma cells as revealed by LC-based metabolomics

Mei-Ling Cheng [a,b], Ming-Shi Shiao [c], Daniel Tsun-Yee Chiu [a,b], Shiue-Fen Weng [a], Hsiang-Yu Tang [a], Hung-Yao Ho [a,*]

[a] Department of Medical Biotechnology and Laboratory Science, Chang Gung University, 259, Wen-Hwa 1st Rd., Kwei-San, Tao-Yuan, Taiwan
[b] Department of Clinical Pathology, Chang Gung Memorial Hospital, Tao-Yuan, Taiwan
[c] Department of Biomedical Sciences, Chang Gung University, Tao-Yuan, Taiwan

ARTICLE INFO

Article history:
Received 5 June 2011
Accepted 29 July 2011
Available online 6 August 2011

Keywords:
Metabolomics
Dehydroepiandrosterone
Mitochondria
s-Adenosylmethionine
Oxidative stress

ABSTRACT

DHEA is known to have chemopreventive and antiproliferative activities, and was initially thought to be mediated by inhibition of G6PD. Our previous study has shown that DHEA may act through interference with energy metabolism. To study the effect of pharmacological dose of DHEA on cellular metabolism, and to further delineate the mechanism underlying its antiproliferative effect, we applied a metabolomic approach to globally profile the changes in metabolites in SK-Hep1 cells underexpressing G6PD (Sk-Gi) and control cells (Sk-Sc) after DHEA treatment. RRLC-TOF-MS was used to identify metabolites, and tandem mass spectrometry was used to confirm their identity. DHEA induced changes in glutathione metabolism, lipid metabolism, *s*-adenosylmethionine (SAM) metabolism, as well as lysine metabolism. Elevation in level of glutathione disulfide, together with a concomitant decrease in level of reduced glutathione, was indicative of increased oxidative stress. Depletion of carnitine and its acyl derivatives reflected decline in fatty acid catabolism. These changes were associated with mitochondrial malfunction and reduction in cellular ATP content. Cardiolipin (CL) and phosphatidylcholine (PC) levels decreased significantly, suggesting that alterations in lipid composition are causally related to decline in mitochondrial function after DHEA treatment. The decline in cellular SAM content was accompanied by decreased expression of methionine adenosyltransferase genes *MAT2A* and *MAT2B*. SAM supplementation partially rescued cells from DHEA-induced growth stagnation. Our findings suggest that DHEA causes perturbation of multiple pathways in cellular metabolism. Decreased SAM production, and cardiolipin depletion and the resulting mitochondrial dysfunction underlie the antiproliferative effect of DHEA.

1. Introduction

DHEA is a steroid secreted by adrenal cortex, gastrointestinal tract, gonads, and brain [1]. DHEA, together with its sulfated form, is the most abundant steroid in human circulation. Its plasma concentration increases during adolescence; reaches its maximum at around 25 years of age; and decreases to about 10% of the adolescent level by the age of 80 [2]. Being a multifunctional hormone, DHEA has beneficial effects such as antiobesity [3,4], lowering of blood sugar [4–6], anti-atherosclerosis [7,8], and memory enhancement [9]. Low DHEA level is also associated with increased risks of tumorigenesis [10,11]. It has been shown that DHEA prevents spontaneous tumorigenesis in p53-nullizygous mice [12], and suppresses chemically-induced carcinogenesis in liver [13–15], colon [16], lung [17], and breast [18]. DHEA exerts growth-inhibitory effect on a number of cell lines *in vitro* [19–21]. As compared with the doses of DHEA used in the studies that demonstrate beneficial effects of DHEA, those used in chemoprevention or growth inhibition studies are relatively high [21–26]. For instance, DHEA has antiobesity effect in castrated rats [27], and beneficial effect in diabetic mice [5,28], when administered orally in the dosage range of 240–520 mg/kg/day; DHEA inhibits the

Abbreviations: BPC, base peak chromatogram; DHEA, dehydroepiandrosterone; ESI, electrospray ionization; G6PD, glucose 6-phosphate dehydrogenase; GSH, glutathione; GSSG, glutathione disulfide; H_2DCF-DA, 2′7′-dihydrodichlorofluorescein diacetate; PCA, principal component analysis; ROS, reactive oxygen species; RRLC-TOF-MS, rapid resolution liquid chromatography coupled with electrospray time-of-flight mass spectrometry; SAM, *s*-adenosylmethionine; Sk-Gi, SK-Hep1 cells expressing G6PD shRNA; Sk-Sc, SK-Hep1 cells expressing scrambled control shRNA.

* Corresponding author. Tel.: +886 3 2118449.
E-mail addresses: chengm@mail.cgu.edu.tw (M.-L. Cheng), msshiao@mail.cgu.edu.tw (M.-S. Shiao), dtychiu@mail.cgu.edu.tw (D.-Y. Chiu), zp0707@mail.cgu.edu.tw (S.-F. Weng), m9605022@stmail.cgu.edu.tw (H.-Y. Tang), hoh01@mail.cgu.edu.tw (H.-Y. Ho).

0006-2952/$ – see front matter © 2011 Elsevier Inc. All rights reserved.
doi:10.1016/j.bcp.2011.07.104

development of atherosclerosis when given at a dose of 125 mg/kg/day [7]. However, DHEA is protective against colorectal cancer, pancreatic cancer and mammary cancer when administered at doses ranging from 1200 to 8000 mg/kg/day [24–26]. DHEA is effective at doses in the hundreds of μM range in *in vitro* growth inhibition studies [19,21]. Using cellular model, we studied the effect of a relatively high dose of DHEA on cellular metabolism, and examined how such changes are causally related to the growth inhibitory effect of DHEA.

Several mechanisms of the antiproliferative effect of DHEA have been proposed. DHEA may act as an uncompetitive inhibitor of glucose-6-phosphate dehydrogenase (G6PD), the rate-limiting enzyme of pentose phosphate pathway, and reduces the supply of NADPH and ribose-5-phosphate. Both of these products are essential to cell growth [29]. However, the role of G6PD in DHEA-induced growth inhibition is questionable [30–34]. We and others have shown that DHEA treatment increased intracellular G6PD activity in hepatoma cell line [35], and promyelocytic leukemia cells [34]. Another mechanism for the growth suppressive effect of DHEA is inhibition of 3-hydroxy-3-methylglutaryl CoA reductase (HMGR). However, we found that addition of mevalonate did not rescue cells from growth cessation [35], excluding the involvement of HMGR as primary target of DHEA. Our previous study also showed that DHEA may affect energy metabolism. However, a complete picture of how DHEA alters metabolic pathways is still lacking. Such information is critical to a thorough understanding of the antiproliferative and chemopreventive actions of DHEA.

Analyses of global changes in metabolic pathways depend on recent advances in high throughput metabolite profiling [36]. Such approach, known as metabolomics, is based on either nuclear magnetic resonance (NMR) spectroscopy or mass spectrometry (MS) [37–39], and allows ones to globally determine the concentration changes of small biological molecules in cells, tissues and biofluids [40,41]. It is particularly helpful for the functional understanding of biological system, as changes in metabolites represent the almost downstream events of transcriptomic and proteomic changes, and are the most reliable indicators of cellular and organismal physiology [42,43]. Application of metabolomic technologies has led to appreciable advances in such fields as cancer biology [44,45], biomarker discovery [45–47], and pharmaceutical development [48,49]. A global metabolomic analysis is essential to the thorough understanding of biochemical actions of DHEA, and hence the mechanism underlying its growth inhibitory effect.

In the present study, we analyzed the metabolome of DHEA-treated hepatoma cells using rapid resolution liquid chromatography (RRLC) coupled with time-of-flight (TOF) mass spectrometry. To study the metabolic pathways related to DHEA-mediated growth inhibition, we examined the corresponding changes in metabolomes of Sk-Gi (underexpressing G6PD) and Sk-Sc (with normal G6PD expression level) cells. Levels of various hydrophilic metabolites changed upon DHEA treatment. These metabolites are associated with glutathione metabolism, lipid metabolism, *s*-adenosylmethionine metabolism, and lysine metabolism. Notably, the level of glutathione disulfide increased, while those of carnitine and acyl derivatives declined. It was associated with a reduction in cellular ATP level. Such changes are suggestive of disturbances in mitochondrial metabolism and redox homeostasis. Indeed, DHEA induced cardiolipin depletion and mitochondrial dysfunction. Moreover, SAM depletion was associated with decreased expression of *MAT2A* and *MAT2B*. Supplementation of DHEA-treated cells with SAM significantly increased their growth rate. Taken together, these results unequivocally indicate that DHEA causes mitochondrial malfunction and disturbances in the metabolic pathways and network, and eventually leads to growth cessation.

2. Materials and methods

2.1. Chemicals and reagents

Unless otherwise stated, DHEA and all other chemicals were obtained from Sigma-Aldrich (St. Louis, MO). Solvents for LC–MS application, such as acetonitrile, methanol, and water, are of CHROMASOLV grade, and were purchased from Sigma–Aldrich (St. Louis, MO). Metabolite standards were available from Sigma–Aldrich. Dulbecco's modified Eagle medium (DMEM), fetal calf serum (FCS), penicillin, streptomycin, amphotericin, and trypan blue were purchased from Invitrogen (Carlsbad, California). 5,5′,6,6′-tetrachloro-1,1′,3,3′-tetraethylbenzimidazolocarbo-cyanine iodide (JC-1) (Molecular Probes, Eugene, OR), dihydrodichlorofluorescein diacetate (H_2DCF-DA) and Hoechst dye were available from Invitrogen (Carlsbad, California).

2.2. Cell culture

Sk-Gi and Sk-Sc cells were derived from SK-Hep-1 cells (ATCC catalog number: HTB-52) by transduction with retroviral vectors encoding G6PD and scrambled control short hairpin RNA (shRNA), respectively. The former shRNA is highly specific against G6PD, while the latter is a validated negative control. [50,51]. These cells were maintained in Dulbecco's modified Eagle's medium (DMEM)/5% fetal calf serum at 37 °C in a humidified atmosphere of 5% CO_2. For DHEA treatment, 2×10^5 cells were incubated with 200 μM DHEA for the indicated period. Cell number was determined by cell counting as well as neutral red assay. The neutral red assay was performed as previously described [35].

2.3. Sample extraction

For extraction of hydrophilic metabolites, the cells were washed twice with phosphate-buffered saline (PBS), and scraped on ice in 1 ml of 80% methanol. The cell lysate was centrifuged at 14,000 × *g* for 15 min at 4 °C, and supernatant was retained for RRLC–TOF-MS analysis. For extraction of lipids, a modification of Folch's method was employed [52]. Briefly stated, the cells were washed twice with PBS, harvested by scraping, and resuspended in 1 ml of PBS. After centrifugation, the pelleted cells were mixed with 100 μl of water, and the suspension was transferred to a glass tube. Six milliliters of chloroform/methanol (2:1, v/v) solution and 1.5 ml of water were added. The sample was vortexed 4 times for 30 s, and subsequently centrifuged at 700 × *g* for 30 min at 4 °C. The upper phase was removed as completely as possible, and the lower phase was sonicated for 10 min. The sample was centrifuged at 700 × *g* for 10 min at 4 °C. The upper phase was removed as completely as possible, and the lower phase was allowed to stand still at 4 °C. Three milliliters of this sample was dried under nitrogen gas, and stored at −80 °C. Prior to analysis, the sample was dissolved in 300 μl of 50% acetonitrile.

2.4. RRLC separation

Chromatographic separation was performed on an Acquity UPLC HSST3 reversed phase C18 column (2.1 mm × 100 mm, particle size of 1.8 μm) (Waters Corp, Milford, MA) using an Agilent 1200 rapid resolution liquid chromatography system (Agilent Technologies, CA, USA), which is equipped with a binary pump, a vacuum degasser, an autosampler, and a thermostatted column compartment. For metabolite profiling, the mobile phase was constituted of 0.1% formic acid (solvent A) and 0.1% formic acid/acetonitrile (solvent B). The mobile phase condition was: solvent A, 2 min; gradient from 0% to 40% solvent B, 4 min; 40% solvent B, 2 min; gradient from 40% to 98% solvent B, 2 min; 98%

solvent B, 6 min; gradient from 98% to 0% solvent B, 2 min. The column temperature was maintained at 40 °C, and the flow rate was 0.25 μl/min. For analysis of lipids, the mobile phase was constituted of 2 mM ammonium formate (solvent A) and acetonitrile (solvent B). The mobile phase condition was: gradient from 45% to 75% solvent B, 6 min; gradient from 75% to 98% solvent B, 24 min; 98% solvent B, 70 min; gradient from 98% to 45% solvent B, 1 min; 45% solvent, 19 min. The column temperature was maintained at 50 °C, and the flow rate was 0.3 ml/min.

2.5. ESI–TOF-MS

The RRLC system was coupled to an Agilent 6510 Q-TOF MS, equipped with an electrospray ionization source. The ESI source was tuned to obtain an average maximum intensity of the precursor ions. For metabolite profiling, positive ion mode was adopted. The nitrogen nebulizer pressure was set at 30 psi and nitrogen drying gas was set at 350 °C with a flow rate of 10 l/min. The capillary and skimmer voltages were set at 4000 V and 65 V, respectively. Data was acquired over the range from m/z 50 to m/z 1000 at a rate of 1 scan per second. Data were stored in profile mode. Positive and negative ion modes were used for analysis of phospholipid metabolites with positively and negatively charged head groups, respectively. Instrumental settings were similar to those described above, with the exception that the mass range from 50 to m/z 1700 was set for negative ion mode. The mass accuracy was automatically calibrated by continuous introduction of internal reference mass ions such as purine ($[M + H]^+$ = 121.050873), hexakis (1H,1H,3H-tetrafluoropropoxy) phosphazine ($[M + H]^+$ = 922.009798), or purine ($[M - H]^-$ = 119.036320) and formate adduct ($[M - H]^-$ = 966.000725). Data were collected using Agilent MassHunter Workstation Data acquisition software.

2.6. Data processing

Individual components in sample (i.e. molecular features) were identified using the Molecular Feature Extraction (MFE) algorithm of MassHunter software. Processing of raw data files resulted in time-aligned ion features (isotopes, adducts and dimers). The algorithm also gave the monoisotopic neutral mass, retention time and ion abundance for each molecular feature. Agilent GeneSpring-MS (Agilent Technologies, CA, USA) was used for analysis and visualization of datasets in numerical data matrices, which represent metabolite concentrations. Principal components analysis (PCA) was applied for clustering and correlation analyses. The relative concentrations of metabolites were compared by ANOVA with Tukey HSD correction. Multivariate data analysis and data representation were all performed by the same software. Volcano plot analysis was also performed. Accurate masses of features showing significant differences between control and test groups were searched against the METLIN, HMDB, and KEGG databases [53–55]. Empirical formulae of compounds were computed by Molecular Formula Generator (MFG) algorithm (Agilent Technologies, CA, USA).

2.7. Metabolite identification and validation

For confirmation of metabolite identity, samples were run under chromatographic conditions similar to those of profiling studies. Mass spectrometric analyses were performed using an Agilent 6510 QTOF MS under the following conditions: gas temperature set at 350 °C; flow rate of drying gas at 10 l/min; nebulizer pressure at 30 psi, capillary voltage at 4000 V; fragmentor voltage at 120 V; and skimmer voltage at 65 V. MS spectra were acquired at a rate of 1 spectra per second, and MS/MS spectra were collected at a rate of 1 spectra per second, with a medium isolation window (~4 m/z). Depending on the nature of compounds, the collision energy was either fixed at 15 V or ramped from 5 V to 35 V.

2.8. Confocal microscopy

The mitochondrial membrane potential was assessed using the cationic, lipophilic dye JC-1. Cells were grown on glass bottom culture dish (MatTek, MA, USA). They were loaded with 0.5 μM JC-1 under condition as described above, and counterstained with 5 μg/ml of Hoechst 33342 ten minutes before examination under Zeiss LSM 510 Meta system (Carl Zeiss MicroImaging GmbH, Heidelberg, Germany). Confocal fluorescence images of JC-1 labeled cells were obtained using Plan-Apochromat 100 × 1.40 NA oil immersion objective. During scanning of JC-1 monomeric form, we used 488 nm excitation line of argon laser, main dichroic beam splitter (HFT 405/488/561/633/KP720), and an emission window set at 505–550 nm. During scanning of JC-1 aggregated form, we used 561 nm excitation line of DPSS laser and an emission window set at 575–615 nm. For scanning of Hoechst dye, we used 405 nm excitation line of diode laser and an emission window set at 420–480 nm. The images were analyzed with Zeiss Zen software package (Carl Zeiss MicroImaging GmbH, Heidelberg, Germany).

The MitoTracker Red staining was performed as previously described [56]. Cells were cultured on glass bottom culture dish (MatTek, MA, USA). They were loaded with 100 nM MitoTracker Red for 20 min at 37 °C, and counterstained with 5 μg/ml of Hoechst 33342 before examination under Zeiss LSM 510 Meta system (Carl Zeiss MicroImaging GmbH, Heidelberg, Germany). Confocal fluorescence microscopy was carried out as described in the preceding section. The only exception was that the MitoTracker Red-stained cells were illuminated with 561 nm excitation line of DPSS laser, and the emission window was set at 575–615 nm.

2.9. Detection of ROS

Intracellular ROS production was assessed using 2′,7′-dihydrodichlorofluorescein diacetate (H_2DCF-DA) [56,57]. Briefly stated, cells were seeded in a 6-well plate at a density of 4×10^4 cells per well. After specified treatment, the cells were washed with PBS and incubated with 20 μM H_2DCF-DA for 30 min at 37 °C. The loaded cells were washed twice with PBS, and trypsinized for flow cytometric analysis. The mean fluorescence intensity (MFI) of dichlorofluorescein (DCF) channel was quantified using CellQuest Pro software (Becton Dickinson, CA, USA).

2.10. Determination of G6PD activity and ATP level

G6PD activity and ATP level were measured as described previously [35].

2.11. Determination of MAT gene expression by quantitative PCR

Total RNA from about 1×10^6 cells were extracted with TRIzol (Invitrogen), according to the manufacturer's instructions. One μg of total RNA was reverse-transcribed into cDNA using RevertAid™ H Minus First Strand cDNA Synthesis Kit (Fermentas). One μl of a 1:100-dilution of the cDNA reaction was subject to quantitative PCR analysis of *MAT* transcript with SYBR® Green PCR Master Mix (Applied Biosystem, Foster City, CA). Respective forward and reverse primers for *MAT1A* gene are: 5′-GGTGTCACTGGCCGTAAGAT-3′ and 5′-GGCATAGGAAACCTGGACAA-3′; those for *MAT2A* gene are: 5′-TTCCCATCAGAGTCCACACA-3′ and 5′-ATTTTGCGTCCAGTCAAACC-3′; those for *MAT2B* gene are: 5′-ACAGAGAGGAAGACATACCAG-3′ and 5′-GTTCATTGCCAGACCAGTG-3′; those for internal calibrator, ribosomal protein L13 gene, are: 5′-CTGAAGGAGTACCGCTC-CAAACT-3′ and 5′-CAGCAGAACTGTCTCCCTTCT TG-3′.

2.12. Statistical analysis

Results are shown as mean ± SD. The mass spectrometry data were analyzed as mentioned in the preceding section. Other data were analyzed by one-way analysis of variance (ANOVA) and Student's *t*-test where appropriate. A *P* value of less than 0.05 is considered significant.

3. Results

3.1. DHEA inhibits growth of SK-Hep1 cells irrespective of G6PD status

To study whether the growth inhibitory effect is mediated via G6PD, we established two cell lines Sk-Gi and Sk-Sc cells, which differed in G6PD expression and activity. The expression and activity of G6PD in Sk-Gi cells were significantly reduced as compared to that of Sk-Sc cells (0.03 ± 0.01 U/mg in Sk-Gi cells vs. 0.29 ± 0.01 U/mg in Sk-Sc cells). When their growth kinetics was examined, Sk-Gi and Sk-Sc cells did not display significant differences in growth rate (Fig. 1A). DHEA treatment inhibited growth of these cells to the same extent. Moreover, DHEA caused dose-dependent increase in cellular G6PD activities of Sk-Sc and Sk-Gi cells (Fig. 1B). These findings indicate that the growth inhibitory effect of DHEA is independent of G6PD activity.

3.2. Metabolomic approach for characterization of DHEA-induced growth inhibition

To identify the metabolic pathways implicated in the mechanism of DHEA-induced growth inhibition, we studied the changes in metabolites common in growth-inhibited Sk-Gi and Sk-Sc cells. The extracts of DHEA-treated cells were analyzed by RRLC–ESI-TOF-MS operating in positive ion mode. Representative base peak chromatograms are shown in Fig. 2.

The abundances of metabolites were subject to multivariate and univariate statistical analysis. A total of 1515 features were identified by MFE algorithm of Agilent MassHunter Qual software. A feature is defined as a unique *m*/*z* chromatographic retention time data for which a peak was present in at least one sample and intensity was measured. Datasets for Sk-Sc cells, Sk-Gi cells, and their DHEA-treated counterparts were analyzed by GeneSpring MS software. The representative points of cell extracts from various experimental groups were mapped in space defined by the principal component 1 and the orthogonal principal component 2. The score plot showed clustering of Sk-Gi and Sk-Sc groups with

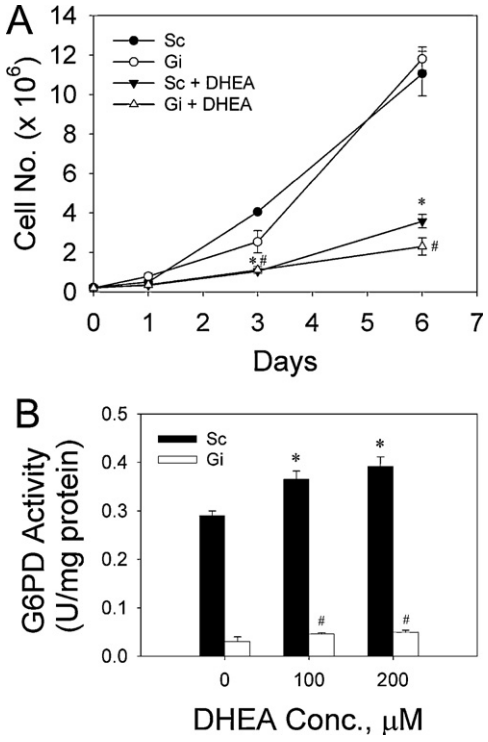

Fig. 1. The growth inhibitory effect of DHEA was irrespective of G6PD status. (A) About 2×10^5 cells were seeded overnight, and treated without or with 200 μM DHEA for indicated time. Cells number at indicated timepoints was determined by neutral red assay. The absorbance values were calibrated to the cell number standard curve. Results are mean ± SD, $n = 3$. $^*p < 0.05$ and $\#p < 0.05$ vs. untreated Sk-Sc and Sk-Gi cells at the corresponding timepoint respectively. (B) Sk-Gi and Sk-Sc cells were treated with indicated concentrations of DHEA for 48 h, and harvested for G6PD activity assay. G6PD activity is given in U/mg of protein in cell lysate. Results are mean ± SD, $n = 6$. $^*p < 0.05$ and $\#p < 0.05$ vs. untreated Sk-Sc and Sk-Gi cells respectively.

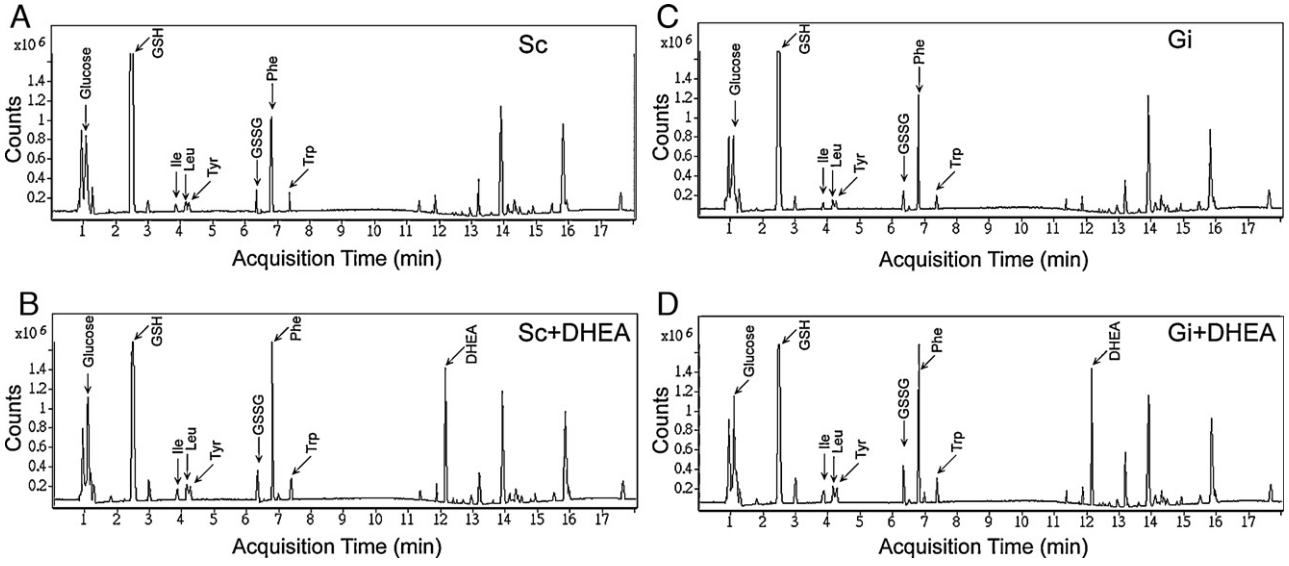

Fig. 2. Base peak chromatograms (BPC) from extracts of Sk-Gi and Sk-Sc cells with or without DHEA treatment. Sk-Sc (A, B) and Sk-Gi (C, D) cells were un- (A, C) or treated (B, D) with 200 μM DHEA. Forty-eight hours later, cells were harvested for RRLC/MS analysis. BPCs from one out of 12 experiments are shown here. *Arrowheads* indicate changes in BPC pattern. Peaks corresponding to glucose, GSH, isoleucine, leucine, tyrosine, GSSG, phenylalanine, tryptophan and DHEA are shown.

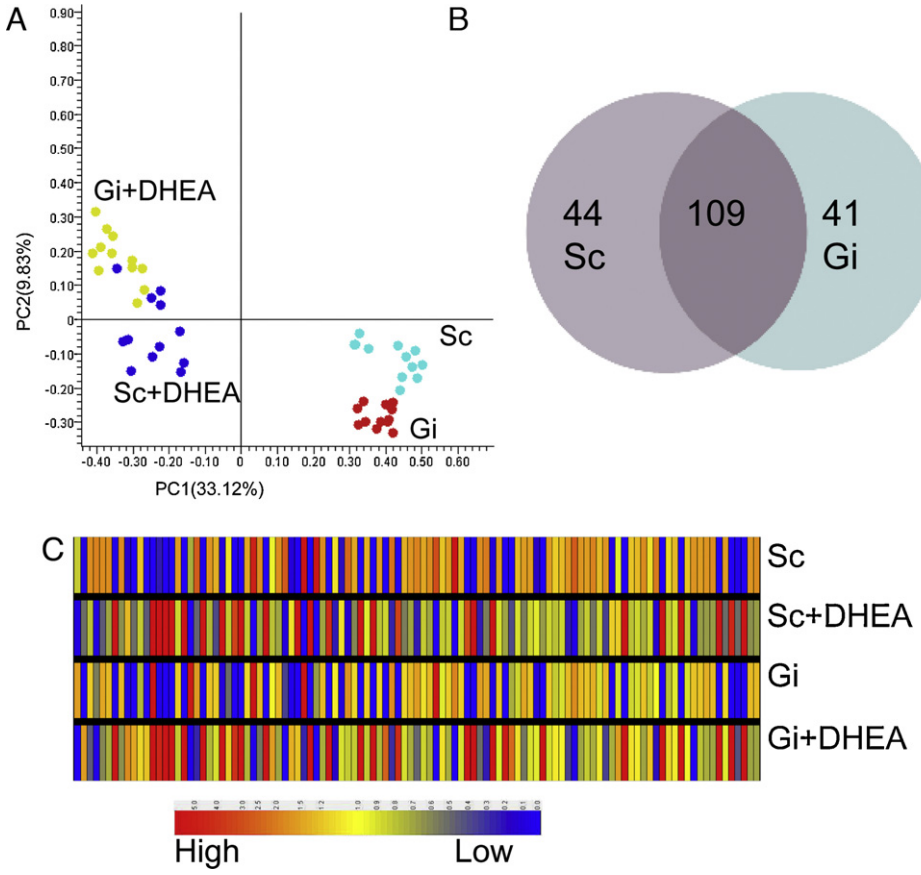

Fig. 3. Principal component analysis (PCA) of metabolomes of Sk-Gi and Sk-Sc cells with or without DHEA treatment. Sk-Gi and Sk-Sc cells were un- or treated with 200 μM DHEA. Cells were harvested for RRLC/MS analysis, and features were acquired in ESI positive ion mode. These features were analyzed by PCA, and PCA score plot is shown (Sk-Gi cells, red filled circle; Sk-Sc cells, cyan filled circle; Sk-Gi cells treated with DHEA, yellow filled circle; Sk-Sc cells treated with DHEA, blue filled circle)(A). The proportions of the first and second PCs (PC1 and PC2) were 33.12% and 9.38%, respectively. (B) The Venn diagram shows the number of metabolites that changed their abundance in Sk-Gi and Sk-Sc cells upon DHEA treatment. (C) Heat map shows the fold-change in abundance of metabolites (i.e. 109) that varied in both Sk-Gi and Sk-Sc datasets.

or without DHEA treatment. The Sk-Gi or Sk-Sc groups with DHEA treatment were well separated from the corresponding groups without treatment. However, Sk-Gi groups were not well distinguished from the Sk-Sc groups receiving the same treatment (Fig. 3A). Such findings advocate the notion that the growth inhibitory effect of DHEA is independent of cellular G6PD status.

Features present in all replicates within these experimental groups were selected and subject to one-way ANOVA analysis. One hundred and nine features showed significant differences in their levels in both Sk-Gi and Sk-Sc cells upon treatment (Fig. 3B). These features, which represent unique metabolites, are illustrated by heat map (Fig. 3C). Consistent with PCA analysis, Sk-Gi and Sk-Sc groups showed similar distribution of signal intensities, which indicate cellular metabolite concentrations. Likewise, DHEA treatment groups had similar signal distribution.

A list of metabolites was generated, and is shown in Tables 1A–1E and Supplementary Table 1. Their identity was validated by acquisition of MS/MS spectra of these metabolites. Their fragmentation patterns were compared with those of the corresponding pure compounds, which were subject to RRLC/MS/MS analysis under identical conditions as the test metabolites.

3.3. Mapping of metabolites onto biochemical pathways

The metabolites of interest were mapped onto biochemical pathways with the help of algorithms available through KEGG and HMDB databases (Fig. 4). Different categories of metabolites changed in their abundances in cells after DHEA treatment (Tables 1A–1E). These include compounds related to lipid metabolism (Table 1A), glutathione metabolism (Table 1B), *s*-adenosylmethionine (SAM) metabolism (Table 1C), and lysine metabolism (Table 1D). Under the first category, cellular levels of phosphocholine, glycerophosphocholine, carnitine, acetylcarnitine and butylcarnitine decreased, while choline increased modestly. Of the metabolites related to glutathione (GSH), levels of γ-glutamylcysteine, glutathione disulfide (GSSG) and pyroglutamic acid (5-oxoproline) increased, while levels of glutathione and glutamate declined. Under the category of SAM-related metabolites, levels of SAM, methylthioadenosine, and spermine were reduced. Moreover, lysine and intermediates in lysine metabolism, such as saccharopine and pipecolate, accumulated after DHEA treatment. Glucose, pantothenic acid, branched-chain and aromatic amino acids also increased in their levels after DHEA treatments (Table 1E). The identity of all these species was validated by MS/MS analyses and comparison to standard reference compounds. A complete list of validated metabolites is provided (Supplementary Table 1).

3.4. DHEA induces oxidative stress in Sk-Gi and Sk-Sc cells

Disturbance of glutathione metabolism and accumulation of GSSG is indicative of increased oxidative stress in DHEA-treated cells. As reported previously [51], the GSH level was lower, but GSSG level was higher in cells expressing shRNA against G6PD than in cells expressing scrambled control shRNA (Fig. 5A and B). DHEA caused oxidative stress in both Sk-Gi and Sk-Sc cells in a time-dependent manner (Fig. 5D). It was accompanied by over 60% reduction in GSH/GSSG ratio in these cells (Fig. 5C).

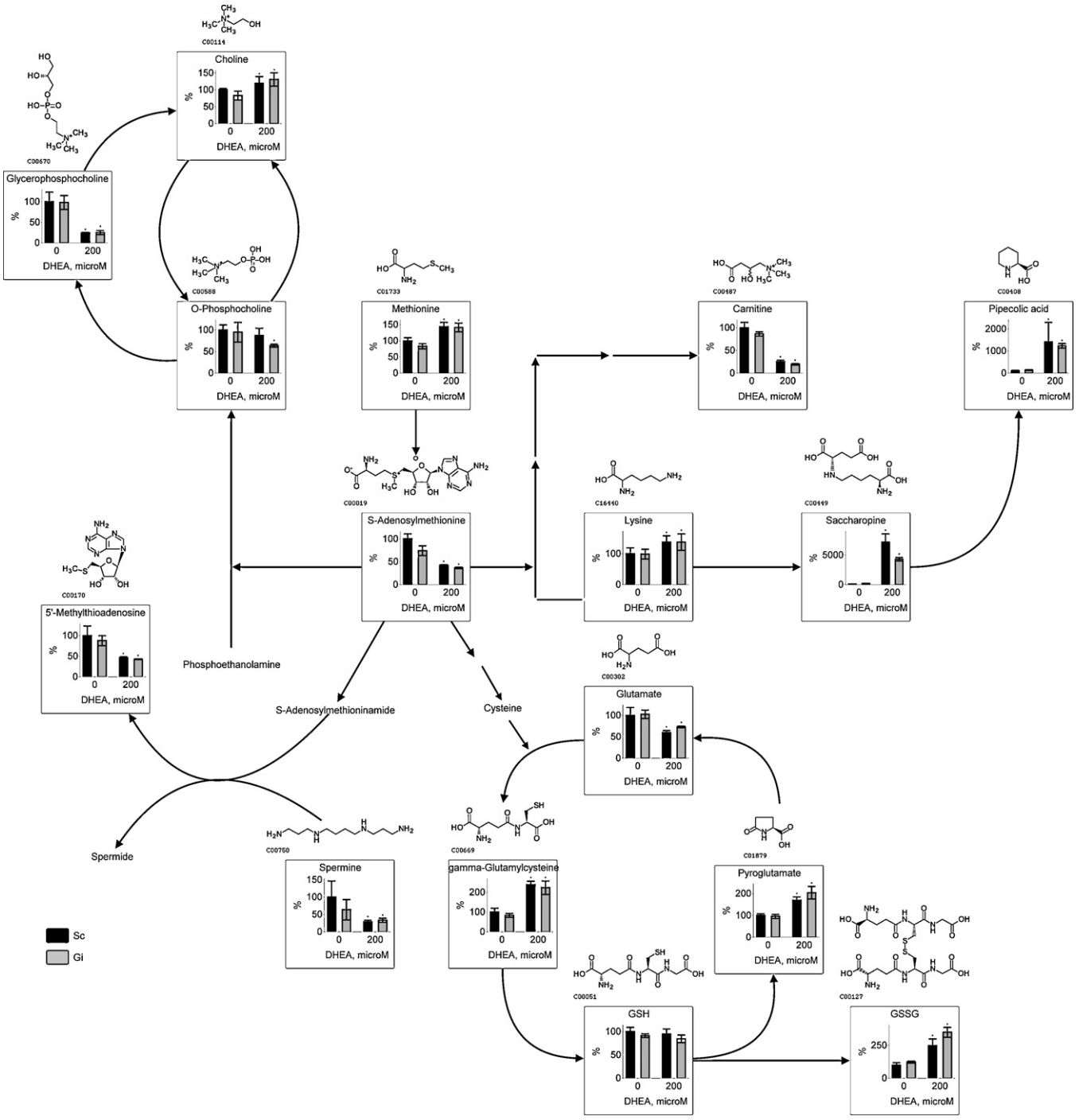

Fig. 4. Metabolite changes mapped onto the pathways involved in DHEA-mediated growth inhibition. Metabolites, as depicted in Table 1, are mapped. The levels of metabolites are expressed as percentage relative to those in untreated Sk-Sc cells. Results are mean ± SD, $n = 12$. $^{*}p < 0.05$ vs. untreated cells.

3.5. DHEA causes phosphocholine and phosphatidylcholine depletion

Phosphocholine and SAM are essential to biosynthesis of phosphatidylcholine (PC). It is possible that DHEA-induced reduction in the cellular content of phophocholine and SAM could lead to depletion of phosphatidylcholine. To test such hypothesis, we extracted cellular lipids using Folch's method. Samples were analyzed by RRLC–ESI-TOF-MS in positive ion mode. Five $[M + H]^+$ ions with m/z 706.5426, 730.5424, 734.5729, 758.5780, and 786.604, which showed significant differences, were identified by MS/MS (Supplementary Fig. 1). In the low-mass region of MS/MS spectra, a fragment ion of m/z 184.07 corresponding to phosphocholine was observed (Supplementary Fig. 2). Comparison of MS/MS spectral data with reference spectra confirms the identity of these metabolites as phosphatidylcholines. The tentative formulae of these phosphatidylcholines are given in Table 2. The abundances of these species were assessed from extracted ion chromatograms. As shown in Table 2, DHEA treatment resulted in significant decrease in levels of these molecules.

3.6. Mitochondria malfunction in DHEA-treated cells

As a major lipid constituent of mitochondria, phosphatidylcholine accounts for 35–50% of mitochondrial phospholipids [58–60].

Table 1A
Changes in metabolites related to lipid metabolism.

Metabolite	Sk-Sc	Sk-Sc treated with DHEA	Sk-Gi	Sk-Gi treated with DHEA
Choline* $C_5H_{14}NO$	1.00 ± 0.04	1.20 ± 0.19	0.83 ± 0.13	1.31 ± 0.2
Phosphocholine* $C_5H_{15}NO_4P$	1.00 ± 0.12	0.87 ± 0.16	0.95 ± 0.23	0.64 ± 0.04
Glycerophosphocholine* $C_8H_{20}NO_6P$	1.00 ± 0.23	0.24 ± 0.01	0.98 ± 0.17	0.25 ± 0.05
Carnitine* $C_7H_{15}NO_3$	1.00 ± 0.12	0.25 ± 0.04	0.86 ± 0.04	0.19 ± 0.02
Acetylcarnitine* $C_9H_{17}NO_4$	1.00 ± 0.04	0.54 ± 0.09	1.15 ± 0.11	0.61 ± 0.04
Butyrylcarnitine* $C_{11}H_{21}NO_4$	1.00 ± 0.08	0.44 ± 0.09	0.90 ± 0.05	0.42 ± 0.06

The identity of the metabolites was validated by MS/MS. Results are the mean ± SEM of 12 determinations.
* $p < 0.01$ vs. untreated cells.

Table 1B
Changes in metabolites related to glutathione pathways.

Metabolite	Sk-Sc	Sk-Sc treated with DHEA	Sk-Gi	Sk-Gi treated with DHEA
GSH $C_{10}H_{17}N_3O_6S$	1.00 ± 0.09	0.95 ± 0.11	0.91 ± 0.04	0.85 ± 0.08
GSSG* $C_{20}H_{32}N_6O_{12}S_2$	1.00 ± 0.19	2.47 ± 0.52	1.22 ± 0.07	3.49 ± 0.37
Glutamate* $C_5H_9NO_4$	1.00 ± 0.18	0.58 ± 0.02	1.03 ± 0.12	0.75 ± 0.05
γ-Glutamylcysteine* $C_8H_{14}N_2O_5S$	1.00 ± 0.2	2.39 ± 0.17	0.83 ± 0.1	2.23 ± 0.34
Pyroglutamate* $C_5H_7NO_3$	1.00 ± 0.07	1.70 ± 0.15	0.95 ± 0.09	2.04 ± 0.29

The identity of the metabolites was validated by MS/MS. Results are the mean ± SEM of 12 determinations.
* $p < 0.01$ vs. untreated cells.

Table 1C
Changes in metabolites related to sam metabolism.

Metabolite	Sk-Sc	Sk-Sc treated with DHEA	Sk-Gi	Sk-Gi treated with DHEA
Methionine* $C_5H_{11}N_4O_2S$	1.00 ± 0.46	1.44 ± 0.14	0.93 ± 0.08	1.41 ± 0.13
S-Adenosylmethionine* $C_{15}H_{23}N_6O_5S$	1.00 ± 0.11	0.42 ± 0.02	0.74 ± 0.11	0.37 ± 0.02
Methylthioadenosine* $C_{11}H_{15}N_5O_3S$	1.00 ± 0.23	0.46 ± 0.02	0.88 ± 0.12	0.42 ± 0.01
Spermine* $C_{10}H_{26}N_4$	1.00 ± 0.46	0.29 ± 0.04	0.63 ± 0.3	0.33 ± 0.06

The identity of the metabolites was validated by MS/MS. Results are the mean ± SEM of 12 determinations.
* $p < 0.01$ vs. untreated cells.

Table 1D
Changes in metabolites related to lysine catabolism.

Metabolite	Sk-Sc	Sk-Sc treated with DHEA	Sk-Gi	Sk-Gi treated with DHEA
Lysine* $C_6H_{14}N_2O_2$	1.00 ± 0.19	1.38 ± 0.2	0.98 ± 0.16	1.37 ± 0.27
Pipecolic acid* $C_6H_{11}NO_2$	1.00 ± 0.2	14.08 ± 8.93	1.35 ± 0.22	12.33 ± 1.02
Saccharopine* $C_{11}H_{20}N_2O_6$	1.00 ± 0.14	71.97 ± 13.92	1.76 ± 0.3	42.98 ± 2.85
Carnitine* $C_7H_{15}NO_3$	1.00 ± 0.12	0.25 ± 0.04	0.86 ± 0.04	0.19 ± 0.02

The identity of the metabolites was validated by MS/MS. Results are the mean ± SEM of 12 determinations.
* $p < 0.01$ vs. untreated cells.

DHEA-induced decrease in phosphatidylcholine content implies an anomaly in mitochondrial lipid composition. To test this possibility, we studied the effect of DHEA on cardiolipin (CL), which is considered as the signature lipid of mitochondria. The samples were analyzed for the levels of cardiolipin by RRLC–ESI-TOF-MS in negative ion mode. Cardiolipin forms $[M\text{-}H]^-$ and $[M\text{-}2H]^{2-}$ ions, but only the latter was detected within the m/z range of 50 – 1700. The $[M - 2H]^{2-}$ ion with m/z 723.4694 corresponds to $(C18:2)_4$ cardiolipin (unpublished data), which is the predominant cardiolipin species in liver. The levels of $(C18:2)_4$ cardiolipin decreased after DHEA treatment (unpublished data; Table 2).

Cardiolipin is believed to be essential to assembly and functioning of respiratory complex. It is plausible that cardiolipin depletion leads to mitochondrial dysfunction. To examine this

Table 1E
Changes in other metabolites.

Metabolite	Sk-Sc	Sk-Sc treated with DHEA	Sk-Gi	Sk-Gi treated with DHEA
Glucose* $C_6H_{12}O_6$	1.00 ± 0.06	2.12 ± 0.51	0.83 ± 0.07	2.29 ± 0.34
Valine* $C_5H_{11}NO_2$	1.00 ± 0.07	1.54 ± 0.30	0.83 ± 0.11	1.64 ± 0.22
Leucine* $C_6H_{13}NO_2$	1.00 ± 0.08	1.48 ± 0.30	0.84 ± 0.09	1.57 ± 0.13
Isoleucine* $C_6H_{13}NO_2$	1.00 ± 0.08	1.52 ± 0.27	0.86 ± 0.07	1.53 ± 0.18
Phenylalanine* $C_9H_{11}NO_2$	1.00 ± 0.19	1.82 ± 0.51	0.92 ± 0.10	1.74 ± 0.09
Tyrosine* $C_9H_{11}NO_3$	1.00 ± 0.12	1.55 ± 0.32	0.88 ± 0.09	1.64 ± 0.15
Tryptophan* $C_{11}H_{12}N_2O_3$	1.00 ± 0.08	1.43 ± 0.24	0.90 ± 0.08	1.48 ± 0.24
Arginine* $C_6H_{14}N_4O_2$	1.00 ± 0.23	1.40 ± 0.19	0.88 ± 0.14	1.57 ± 0.18
Pantothenic acid * $C_9H_{17}NO_6$	1.00 ± 0.05	2.61 ± 0.39	0.87 ± 0.08	2.73 ± 0.31

The identity of the metabolites was validated by MS/MS. The level of each metabolite is expressed relative to that of untreated Sc cells. Results are the mean ± SEM of 12 determinations.
* $p < 0.01$ vs. untreated cells.

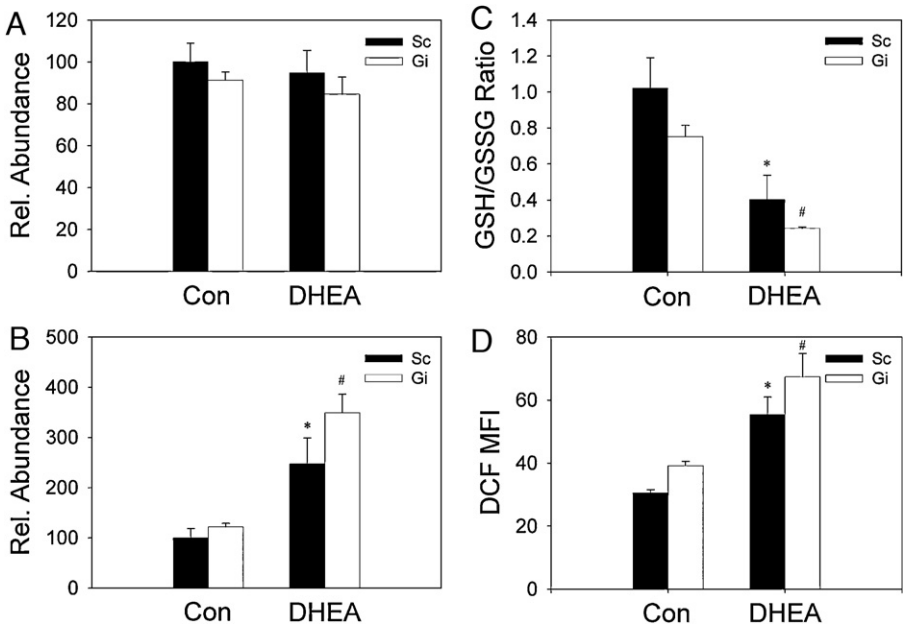

Fig. 5. Increased oxidative stress in Sk-Gi and Sk-Sc cells upon DHEA treatment. (A–C) Sk-Gi and Sk-Sc cells were treated without (*Con*) or with 200 μM DHEA (*DHEA*). Forty-eight hours later, cellular levels of GSH (*A*) and GSSG (*B*) were quantified by RRLC/MS. All these values are expressed relative to those of untreated Sk-Sc cells. The GSH/GSSG ratio (C) was calculated. All these values are expressed relative to those of untreated Sk-Sc cells. Results are mean ± SD, $n = 12$. $^*p < 0.05$ and $\#p < 0.05$ vs. untreated Sk-Sc and Sk-Gi cells respectively. (D) Sk-Gi and Sk-Sc cells were treated without (*Con*) or with 200 μM DHEA (*DHEA*) for 48 h. ROS level was quantified by H_2DCF-DA staining. Results are mean ± SD, $n = 3$. $^*p < 0.05$ and $\#p < 0.05$ vs. untreated Sk-Sc and Sk-Gi cells respectively.

possibility, we employed JC-1 staining and confocal microscopy to assess mitochondrial membrane potential. As shown in Fig. 6, the mitochondria in untreated cells displayed red fluorescence, which is characteristic of energized mitochondria. After incubation with 200 μM DHEA, mitochondria displayed heterogeneity in JC-1 fluorescence: a significant reduction in red fluorescence was concomitant with enhancement of green fluorescence, which is indicative of mitochondrial depolarization (Fig. 6B and D). Mitochondrial malfunction was accompanied by change in their morphology. In the untreated cells, mitochondria were slender tubular structures, and constituted a reticulum (Fig. 6E and G). After treatment with 200 μM DHEA for 48 h, the reticulum appeared to break up, giving rise to clusters of ovoid structures (Fig. 6F and H). The morphologic changes, together with decline in $\Delta\Psi_m$, suggest a change in mitochondrial physiology in DHEA-treated cells.

DHEA-induced mitochondrial dysfunction was associated with reduction in cellular ATP level. As shown in Fig. 7, Sk-Gi and Sk-Sc cells had their ATP level reduced by about 24% and 26%, respectively after treatment with 200 μM DHEA for 48 h.

3.7. DHEA reduces expression of MAT2A and MAT2B genes

The DHEA-induced reduction in SAM levels may reflect a decline in its biosynthesis. To test such possibility, we quantified the expression of methionine adenosyltransferase genes (*MATs*),

Table 2
Changes in lipid metabolites.

Metabolite, *m/z* tentative formulae	Chemical name	Sk-Sc treated with DHEA (% of untreated cells)	Sk-Gi treated with DHEA (% of untreated cells)
1. 730.5424* $C_{40}H_{76}NO_8P$	PC(18:2(9Z,12Z)/14:0);PC(18:1(9Z)/14:1(9Z)) PC(18:1(11Z)/14:1(9Z)); PC(16:1(9Z)/16:1(9Z)) PC(14:1(9Z)/18:1(9Z)); PC(14:1(9Z)/18:1(11Z)) PC(14:0/18:2(9Z,12Z))	29.91	34.51
2. 706.5426* $C_{38}H_{76}NO_8P$	PC(16:0/14:0); PC(14:0/16:0)	68.63	65.75
3. 758.5780* $C_{42}H_{80}NO_8P$	PC(16:0/18:2(9Z,12Z));PC(14:1(9Z)/20:1(11Z)); PC(20:2(11Z,14Z)/14:0);PC(14:0/20:2(11Z,14Z)); PC(20:1(11Z)/14:1(9Z))	57.12	32.22
4. 734.5729* $C_{40}H_{80}NO_8P$	PC(16:0/16:0);PC(18:0/14:0); PC(14:0/18:0)	73.85	60.73
5. 786.604* $C_{44}H_{84}NO_8P$	PC(18:2(9Z,12Z)/18:0); PC(18:1(9Z)/18:1(11Z)) PC(18:1(11Z)/18:1(9Z));PC(18:1(11Z)/18:1(11Z)); PC(18:1(9Z)/18:1(9Z));PC(18:0/18:2(9Z,12Z)); PC(16:1(9Z)/20:1(11Z));PC(22:2(13Z,16Z)/14:0); PC(22:1(13Z)/14:1(9Z));PC(16:0/20:2(11Z,14Z)); PC(14:1(9Z)/22:1(13Z));PC(20:2(11Z,14Z)/16:0); PC(14:0/22:2(13Z,16Z));PC(20:1(11Z)/16:1(9Z))	76.31	55.37
6. 723.4694* $C_{81}H_{142}O_{17}P_2$	CL(18:2(9Z,12Z)/18:2(9Z,12Z)/18:2(9Z,12Z)/18:2(9Z,12Z))	19.74	19.32

Product ion spectra of $[M+H]^+$ ions with *m/z* 730.5424 (1), 706.5426 (2), 758.5780 (3), 734.5729 (4), 786.604 (5), and product ion spectra of $[M-2H]^{2-}$ ion with *m/z* 723.4694 (6), are listed. The corresponding metabolites were quantified from peak areas of extracted ion chromatograms. The identity of PC was validated by MS/MS, and that of cardiolipin was confirmed by the presence of characteristic $[M-2H]^{2-}$ ions. The level of each metabolite is expressed relative to that of untreated cells. $n = 3$.
* $p < 0.05$ vs. untreated cells.

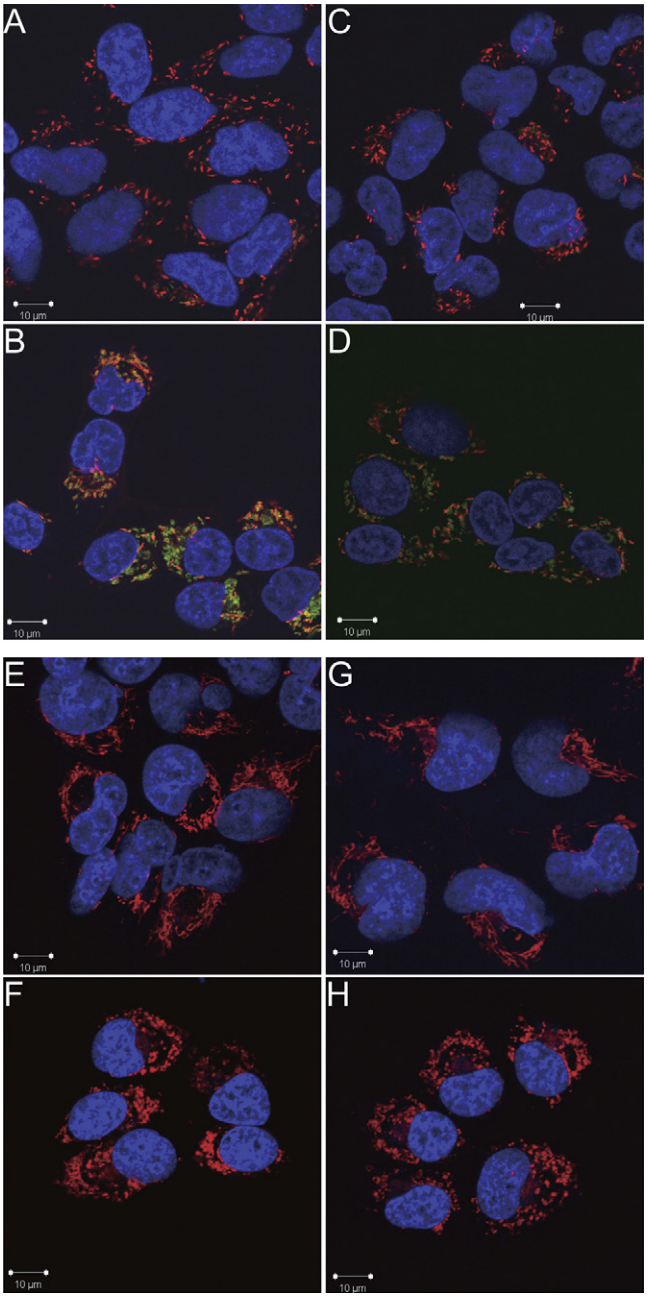

Fig. 6. DHEA induced mitochondrial dysfunction. Sk-Sc (A, B, E and F) and Sk-Gi (C, D, G and H) cells were un- (A, C, E and G) or treated (B, D, F and H) with 200 μM DHEA for 48 h. The cells were stained with JC-1, and analyzed for mitochondrial $\Delta\Psi\mu$ (A–D). The morphology and distribution of mitochondria were analyzed by Mitotracker Red staining (E–H). All the specimens were counterstained with Hoechst 33342 dye. The photographs shown here are representative of three experiments. Scale bar, 10 μm.

including *MAT1A*, *MAT2A* and *MAT2B*, in un- or DHEA-treated Sk-Sc and Sk-Gi cells by quantitative PCR. *MAT1A* encodes polypeptide that makes up catalytically active homodimer and tetradimer, designated MAT III and I, respectively. *MAT2A* and *MAT2B* encode catalytic and regulatory subunits of MAT II. *MAT2A* and *2B* genes were expressed in Gi and Sc cells (Fig. 8). DHEA significantly reduced the expression of *MAT2A* and *2B* genes by more than 50%. However, we were not able to detect the the *MAT1A* transcript by RT-PCR even after 40 cycles of amplification, suggesting that *MAT1A* is not expressed in Sc and Gi cells (data not shown).

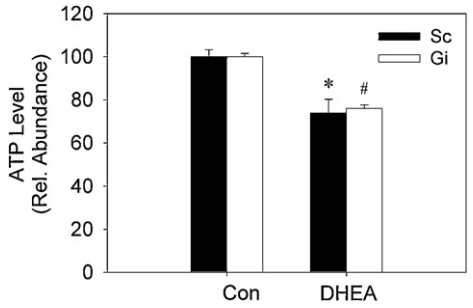

Fig. 7. DHEA treatment caused reduction in cellular ATP content. Sk-Sc and Sk-Gi cells were treated without (*Con*) or with 200 μM DHEA (*DHEA*) for 48 h. Their ATP levels were measured, and are expressed relative to that of untreated Sk-Sc cells. Results are mean ± SD, $n = 3$. $^{*}p < 0.05$ and $\#p < 0.05$ vs. untreated Sk-Sc and Sk-Gi cells respectively.

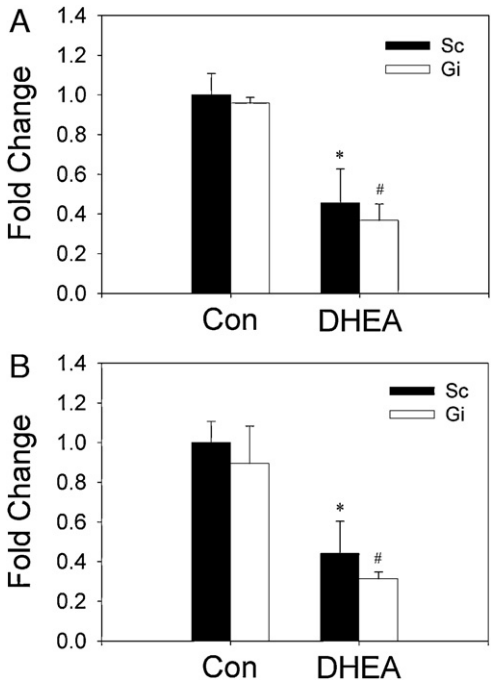

Fig. 8. Expression of *MAT2A* and *2B* gene in DHEA-treated Sc and Gi cells. Sk-Sc and Sk-Gi cells were treated without (*Con*) or with 200 μM DHEA (*DHEA*) for 48 h. Total RNA was extracted, and cDNA was prepared. Expression of *MAT2A* (A) and *MAT2B* (B) genes was quantified by quantitative PCR. The transcript levels are represented as fold change relative to that of untreated Sk-Sc cells. Results are mean ± SD. $n = 3$. $^{*}p < 0.05$ and $\#p < 0.05$ vs. untreated Sk-Sc and Sk-Gi cells respectively.

3.8. SAM ameliorates DHEA-induced growth suppression

To study whether exogenous SAM supplementation can avert DHEA-induced growth stagnation, we pre-treated Sk-Gi and Sk-Sc cells with SAM for 30 min prior to DHEA treatment. Forty-eight hours later, neutral red assay was performed. As shown in Fig. 9, SAM increased the growth of DHEA-treated cells in a dose-dependent manner. At SAM concentration greater than 25 μM, cell growth increased by more than 30%. These findings suggest that SAM biosynthetic pathway is a target of DHEA.

4. Discussion

It is currently unknown how DHEA affects cellular metabolism globally and how such metabolic changes are related to its growth inhibitory effect. In the present study, we have shown that DHEA treatment affected glutathione metabolism, lipid metabolism, SAM

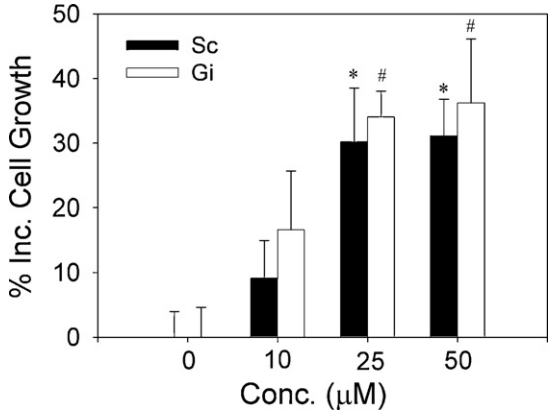

Fig. 9. SAM supplementation partially rescued cells from DHEA-induced growth stagnation. Sk-Sc and Sk-Gi cells were treated with the indicated concentrations of SAM for 30 min prior to addition of 200 μM DHEA. Forty-eight hours later, the cell number was determined as described in the legend of Fig. 1. The percentage increase in growth of SAM-treated cells relative to cells without pre-treatment is shown. Results are mean ± SD, $n = 3$. $^{*}p < 0.05$ and $\#p < 0.05$ vs. Sk-Sc and Sk-Gi cells without pre-treatment respectively.

metabolism, and lysine metabolism. The accumulation of GSSG and increased DCF fluorescence indicated that DHEA-treated cells were under oxidative stress. Reduction in levels of carnitine, phosphatidylcholine and cardiolipin were associated with deleterious changes in mitochondria and energy metabolism. Moreover, reduction in cellular SAM content was associated with decreased expression of *MAT2A* and *MAT2B* genes. Conversely, exogenous SAM supplementation partially reversed the growth inhibitory effect of DHEA. At pharmacological dose of DHEA required for its antiproliferative activity, DHEA disturbs multiple pathways in cellular metabolism, resulting in SAM depletion, mitochondrial dysfunction and increased oxidative stress.

Several lines of evidence suggest that DHEA does not suppress cell growth through inhibition of G6PD. DHEA inhibits proliferation of Sk-Gi and Sk-Sc to a similar extent. Moreover, DHEA treatment increases cellular G6PD activities in Sk-Sc and Sk-Gi cells. Thus, it is likely that G6PD is not the target for growth inhibition by DHEA. Notwithstanding the importance of G6PD in cellular redox homeostasis and antioxidant defense, such findings do not necessarily mean that oxidative stress is not involved in actions of DHEA. Instead, it is probable that the antioxidant defense in Sk-Gi cells is compensated for by alternative pathways, despite a large difference in G6PD activity between Sk-Gi and Sk-Sc cells. After DHEA treatment, ROS generation is induced to more or less similar extent in these cells (i.e. about 1.7-fold increase in DCF fluorescence). Our studies may also give clue to the compensatory pathways in Sk-Gi cells. Sk-Gi cells may rely more on *de novo* GSH synthesis for maintenance of GSH pool. Moreover, we have recently found that NADP synthesis is up-regulated in Sk-Gi cells (unpublished data).

The effect of DHEA on glutathione merits attention. Level of GSSG increased more than 3-fold in DHEA-treated cells, whilst that of GSH declined modestly. This suggests that attenuation of GSH antioxidant defense may not be the primary cause for increased oxidative stress. Instead, the increased rate of reactive oxygen species production by malfunctioning mitochondria may account for oxidative stress. Consistent with this, superoxide anion formation increased in these cells, as shown by the increase in the fluorescence of the MitoSOX red dye-loaded cells upon DHEA treatment (unpublished data). Apparently, DHEA-treated cells up-regulate the synthesis of γ-glutamylcysteine and GSH. It has been recently reported that DHEA induces expression of γ-glutamylcysteine synthetase [61]. Increased glutathione synthesis may cause exhaustion of glutamate. Moreover, excess γ-glutamylcysteine also leads to generation of 5-oxoproline (pyroglutamic acid), possibly via action of γ-glutamylcyclotransferase. These findings suggest that oxidative stress imposes a drain on GSH pool, and cells hasten the γ-glutamylcysteine synthesis in an attempt to restore the GSH homeostasis. These events lead to gradual depletion of glutamate pool.

Accumulation of saccharopine and pipecolate, catabolic products of lysine, suggests that lysine catabolism is enhanced in DHEA-treated cells. It has been reported that expression of lysine-2-oxoglutarate reductase, the first enzyme in lysine degradation pathway, is induced by treatment with glucagon and glucocorticoid in rats [62]. It is possible that DHEA may act in the same way. An alternative but not exclusive possibility is that the catabolism of saccharopine and pipecolate is affected by DHEA, and it needs further clarification.

SAM, as a primary methyl donor in anabolism, is synthesized by MATs. Expression of *MAT2A* and *MAT2B* genes was reduced in DHEA-treated cells, suggesting that DHEA inhibits SAM synthesis through downregulation of MAT II enzyme. This is in agreement with our finding that the SAM levels in Sk-Sc and Sk-Gi cells decreased despite an increase in their methionine levels. It is probable that DHEA may regulate transcription of *MAT2A* and *MAT2B* genes. For instance, transcription of *MAT2A* gene can be regulated through modulation of transcription factors like AP-1 and NF-κB [63], which have been reported as molecular targets of DHEA [64,65]. SAM supplementation partially reversed the DHEA-induced growth inhibition, highlighting the importance of SAM in cell growth. Consistent with this, expression of MAT2B confers growth advantage for hepatoma cells [66]. Suppression of MAT2B expression inhibits growth of hepatoma cells [67].

SAM takes the center stage of cellular metabolism. SAM acts as a precursor for biosynthesis of phosphatidylcholine and cysteine. The latter is required for the synthesis of γ-glutamylcysteine. Depletion of SAM leads to reduction in cellular phosphatidylcholine content. SAM is converted to *s*-adenosylmethioninamine, which is required for synthesis of spermidine and spermine. SAM depletion was associated with decreases in levels of spermine and *s*-methyl-5′-thioadenosine (another product of spermidine synthase and spermine synthase). Paradoxically, spermidine was maintained at a constant level after DHEA treatment. It is possible that DHEA differentially regulates the activities of spermidine synthase and spermine synthase, which accounts for the imbalance in cellular content of polyamines. It has been reported that steroid hormone like testosterone can selectively up-regulate the spermidine synthase activity but not that of spermine synthase [68,69]. Spermine is involved in regulation of transcription factors such as polyamine-modulated transcription factor 1 and Nrf-2; modulates the activity of eukaryotic initiation factor 5A; and regulates functions of ion channels and other signal transducers (reviewed in [70,71]). Spermine is essential to normal cell proliferation: polyamine deficiency causes G1 arrest and delays cell cycle progression [72,73]. Consistent with such notion, decline in spermine in DHEA-treated cells is associated with growth arrest.

SAM plays an important role in synthesis of carnitine. SAM donates its methyl group to lysine residues of protein in a reaction catalyzed by protein-lysine N-methyltransferase. Certain proteins contain trimethyl-lysine residues, which can be released by proteolysis. Trimethyl-lysine serves as precursor for biosynthesis of carnitine [74]. Fatty acids are transferred into mitochondria in the form of acylated carnitine, which is converted into acyl-CoA for β-oxidation. Carnitine helps to remove acyl moieties from mitochondria, and thereby maintains fatty acid homeostasis. Excess free fatty acids induce mitochondrial dysfunction and generation of reactive oxygen species, which can be alleviated by carnitine treatment. Carnitine deficiency compromises mitochondrial functions [75].

A carnitine derivative, acetylcarnitine, serves as an indicator of mitochondrial acetyl-CoA metabolism. Acetyl-CoA, made available through catabolism of pyruvate, amino acid and fatty acids, can be reversibly converted to acetylcarnitine by mitochondrial carnitine acetyltransferase. Acetylcarnitine may be exported to cytosol by carnitine acylcarnitine translocase, and provide acetyl group for synthesis of steroids and fatty acids. Reduction in cellular content of carnitine and acetylcarnitine in DHEA-treated cells reflects anomalous changes in mitochondria and cellular energy metabolism.

Phosphatidylcholine is an important component of cellular membranes. It can be broken down into glycerophosphocholine through consecutive action of phospholipase A2 (or A1) and lysophospholipase I. Glycerophosphocholine is further converted into phosphocholine and choline. Alternatively, phosphatidylcholine can be acted upon by phospholipase C and D to yield phosphocholine and choline, respectively. More than 95% of choline is present as phosphatidylcholine, with the remaining 5% as free choline, phosphocholine and glycerophosphocholine [76]. Changes in levels of choline and its derivatives may represent abnormal turnover of cellular membranes, which include mitochondrial membranes. The change in lipid composition of mitochondrial membrane can change the activity of respirasome. It has been reported that phosphatidylcholine was required for full activity of complex I [77]. Diminution in cellular phosphatidylcholine level may cause mitochondrial dysfunction. There appears to be complicated relationship between mitochondria and phospholipases. Though aberrant lipid metabolism causes mitochondrial impairment, mitochondrial dysfunction may affect phosphatidylcholine metabolism in return. It has been shown that inhibition of complex II and III differentially increased choline at the expense of phosphocholine [78]. It has been postulated that inhibition of respiratory complex specifically modulates activities of phospholipases. Such finding probably explains the selective increase in choline level and decrease in phosphocholine level in cells after DHEA treatment.

As a signature lipid of mitochondria, cardiolipin is a structurally unique phospholipid in the inner mitochondrial membrane. Fatty acid composition of cardiolipin is specific: linoleic acid (C18:2) is a major fatty acid in mammalian tissues, accounting for 80–90% of cardiolipin acyl chains [79]. Tetralinoleoyl $(C18:2)_4$ cardiolipin is the most abundant species [80,81]. Decreased $(C18:2)_4$ cardiolipin content in DHEA-treated cells is indicative of anomalous cardiolipin metabolism. Cardiolipin is essential to maintenance of the structure and activity of mitochondrial electron transport chain complexes [79,82]; it may be involved directly in proton pumping by cytochrome bc_1 complex [83]; cardiolipin helps to tether cytochrome C to inner mitochondrial membrane [84]; and it plays critical roles in assembly of respirasome and mitochondrial biogenesis [85,86]. Given the importance of cardiolipin in normal mitochondrial functioning, its depletion is likely to account for decline in $\Delta\Psi_m$ and the subsequent enhancement of ROS production.

Added to the complexity of this scenario, cardiolipin participates in formation of dynamic membrane domain of high curvature. Its deficiency may change the curvature and hence the morphology of mitochondria [87]. Moreover, phosphatidylcholine provides linoleyl groups for remodeling of cardiolipin via transacylation catalyzed by tafazzin [88]. It is plausible that decrease in phosphatidylcholine content further hampers the biochemical function of cardiolipin. It has been shown that defect in cardiolipin remodeling activity increases the diversity of acyl groups, and leads to abnormal mitochondrial morphology and function [89]. Our findings suggest that DHEA-induced anomaly in phosphatidylcholine and cardiolipin may cause detrimental changes in morphology and functions of mitochondria.

The mitochondrial dysfunction and the resultant ROS generation may have important implications. The increased oxidative stress may in turn affect cellular metabolism. For instance, oxidative stress may lead to reduction in cellular SAM level [90], probably through redox regulation of MAT [91]. In addition, ROS may cause oxidation and loss of phosphatidylcholine and cardiolipin [92,93]. As mentioned earlier, these processes may further adversely affect the cellular metabolism and mitochondrial functions.

In summary, we have applied an unbiased metabolomic approach to delineate the growth inhibitory effect of DHEA. At pharmacological dose of DHEA required for its antiproliferative activity, a number of biochemical pathways, including those involved in glutathione metabolism, lipid metabolism, SAM metabolism, and lysine catabolism, are affected concomitantly. Some of these metabolic changes are associated with mitochondrial dysfunction and reduction in cellular ATP content. Depletion of cardiolipin and phosphatidylcholine may cause abnormalities in mitochondrial structure and functions. All in all, our findings strongly support the notion that DHEA-induced growth retardation is associated with anomalous changes in SAM metabolism, cellular energy metabolism and redox homeostasis.

Acknowledgments

The research work was supported, in whole or in part, by grants from Chang Gung University (CMRPD160233, CMRPD 190421, CMRPG391681, CMRPD160313, CMRPD190441), National Science Council of Taiwan (NSC96-2320-B-182-015-MY3, NSC97-2320-B-182-013-MY3, NSC96-2320-B-182A-003-MY3, NSC99-2320-B-182A-005-MY3, NSC97-2320-B-182-015-MY3) and Ministry of Education of Taiwan (EMRPD190211).

Appendix A. Supplementary data

Supplementary data associated with this article can be found, in the online version, at doi:10.1016/j.bcp.2011.07.104.

References

[1] Parker Jr CR. Dehydroepiandrosterone and dehydroepiandrosterone sulfate production in the human adrenal during development and aging. Steroids 1999;64:640–7.
[2] Yen SS, Laughlin GA. Aging and the adrenal cortex. Exp Gerontol 1998;33:897–910.
[3] Cleary MP. The antiobesity effect of dehydroepiandrosterone in rats. Proc Soc Exp Biol Med 1991;196:8–16.
[4] McIntosh MK, Berdanier CD. Antiobesity effects of dehydroepiandrosterone are mediated by futile substrate cycling in hepatocytes of BHE/cdb rats. J Nutr 1991;121:2037–43.
[5] Coleman DL, Leiter EH, Schwizer RW. Therapeutic effects of dehydroepiandrosterone (DHEA) in diabetic mice. Diabetes 1982;31:830–3.
[6] Coleman DL, Schwizer RW, Leiter EH. Effect of genetic background on the therapeutic effects of dehydroepiandrosterone (DHEA) in diabetes-obesity mutants and in aged normal mice. Diabetes 1984;33:26–32.
[7] Gordon GB, Bush DE, Weisman HF. Reduction of atherosclerosis by administration of dehydroepiandrosterone. A study in the hypercholesterolemic New Zealand white rabbit with aortic intimal injury. J Clin Invest 1988;82:712–20.
[8] Nafziger AN, Herrington DM, Bush TL. Dehydroepiandrosterone and dehydroepiandrosterone sulfate: their relation to cardiovascular disease. Epidemiol Rev 1991;13:267–93.
[9] Wojtal K, Trojnar MK, Czuczwar SJ. Endogenous neuroprotective factors: neurosteroids. Pharmacol Rep 2006;58:335–40.
[10] Zumoff B, Levin J, Rosenfeld RS, Markham M, Strain GW, Fukushima DK. Abnormal 24-hr mean plasma concentrations of dehydroisoandrosterone and dehydroisoandrosterone sulfate in women with primary operable breast cancer. Cancer Res 1981;41:3360–3.
[11] Gordon GB, Helzlsouer KJ, Comstock GW. Serum levels of dehydroepiandrosterone and its sulfate and the risk of developing bladder cancer. Cancer Res 1991;51:1366–9.
[12] Hursting SD, Perkins SN, Haines DC, Ward JM, Phang JM. Chemoprevention of spontaneous tumorigenesis in p53-knockout mice. Cancer Res 1995;55:3949–53.

[13] Moore MA, Thamavit W, Ichihara A, Sato K, Ito N. Influence of dehydroepiandrosterone, diaminopropane and butylated hydroxyanisole treatment during the induction phase of rat liver nodular lesions in a short-term system. Carcinogenesis 1986;7:1059–63.
[14] Garcea R, Daino L, Pascale R, Frassetto S, Cozzolino P, Ruggiu ME, et al. Inhibition by dehydroepiandrosterone of liver preneoplastic foci formation in rats after initiation-selection in experimental carcinogenesis. Toxicol Pathol 1987;15:164–9.
[15] Simile M, Pascale RM, De Miglio MR, Nufris A, Daino L, Seddaiu MA, et al. Inhibition by dehydroepiandrosterone of growth and progression of persistent liver nodules in experimental rat liver carcinogenesis. Int J Cancer 1995;62:210–5.
[16] Nyce JW, Magee PN, Hard GC, Schwartz AG. Inhibition of 1,2-dimethylhydrazine-induced colon tumorigenesis in Balb/c mice by dehydroepiandrosterone. Carcinogenesis 1984;5:57–62.
[17] Schwartz AG, Tannen RH. Inhibition of 7,12-dimethylbenz[a]anthracene- and urethan-induced lung tumor formation in A/J mice by long-term treatment with dehydroepiandrosterone. Carcinogenesis 1981;2:1335–7.
[18] Ratko TA, Detrisac CJ, Mehta RG, Kelloff GJ, Moon RC. Inhibition of rat mammary gland chemical carcinogenesis by dietary dehydroepiandrosterone or a fluorinated analogue of dehydroepiandrosterone. Cancer Res 1991;51:481–6.
[19] Melvin WS, Boros LG, Muscarella P, Brandes JL, Johnson JA, Fisher WE, et al. Dehydroepiandrosterone-sulfate inhibits pancreatic carcinoma cell proliferation in vitro and in vivo. Surgery 1997;121:392–7.
[20] Rao MS, Subbarao V. Dehydroepiandrosterone inhibits DNA synthesis of rat hepatocytes induced by partial hepatectomy or mitogen (ciprofibrate). Cell Prolif 1997;30:1–5.
[21] Lopez-Marure R, Contreras PG, Dillon JS. Effects of dehydroepiandrosterone on proliferation, migration, and death of breast cancer cells. Eur J Pharmacol 2011;660:268–74.
[22] Svec F, Porter JR. The actions of exogenous dehydroepiandrosterone in experimental animals and humans. Proc Soc Exp Biol Med 1998;218:174–91.
[23] Matsuzaki Y, Honda A. Dehydroepiandrosterone and its derivatives: potentially novel anti-proliferative and chemopreventive agents. Curr Pharm Des 2006;12:3411–21.
[24] Klann RC, Holbrook CT, Nyce JW. Chemotherapy of murine colorectal carcinoma with cisplatin and cisplatin plus 3'-deoxy-3'-azidothymidine. Anticancer Res 1992;12:781–7.
[25] Muscarella P, Boros LG, Fisher WE, Rink C, Melvin WS. Oral dehydroepiandrosterone inhibits the growth of human pancreatic cancer in nude mice. J Surg Res 1998;79:154–7.
[26] Green JE, Shibata MA, Shibata E, Moon RC, Anver MR, Kelloff G, et al. 2-difluoromethylornithine and dehydroepiandrosterone inhibit mammary tumor progression but not mammary or prostate tumor initiation in C3(1)/SV40 T/t-antigen transgenic mice. Cancer Res 2001;61:7449–55.
[27] Taniguchi S, Yanase T, Haji M, Ishibashi K, Takayanagi R, Nawata H. The antiobesity effect of dehydroepiandrosterone in castrated or noncastrated obese Zucker male rats. Obesity Res 1995;3(Suppl 5):639S–43S.
[28] Coleman DL, Leiter EH, Applezweig N. Therapeutic effects of dehydroepiandrosterone metabolites in diabetes mutant mice (C57BL/KsJ-db/db). Endocrinology 1984;115:239–43.
[29] Tian WN, Braunstein LD, Pang J, Stuhlmeier KM, Xi QC, Tian X, et al. Importance of glucose-6-phosphate dehydrogenase activity for cell growth. J Biol Chem 1998;273:10609–17.
[30] Boccuzzi G, Di Monaco M, Brignardello E, Leonardi L, Gatto V, Pizzini A, et al. Dehydroepiandrosterone antiestrogenic action through androgen receptor in MCF-7 human breast cancer cell line. Anticancer Res 1993;13:2267–72.
[31] Yoshida S, Honda A, Matsuzaki Y, Fukushima S, Tanaka N, Takagiwa A, et al. Anti-proliferative action of endogenous dehydroepiandrosterone metabolites on human cancer cell lines. Steroids 2003;68:73–83.
[32] Biaglow JE, Ayene IS, Koch CJ, Donahue J, Stamato TD, Tuttle SW. G6PD deficient cells and the bioreduction of disulfides: effects of DHEA, GSH depletion and phenylarsine oxide. Biochem Biophys Res Commun 2000;273:846–52.
[33] Ng HP, Wang YF, Lee CY, Hu ML. Toxicological and antioxidant effects of short-term dehydroepiandrosterone injection in young rats fed diets deficient or adequate in vitamin E. Food Chem Toxicol 1999;37:503–8.
[34] Izumo K, Horiuchi M, Komatsu M, Aoyama K, Bandow K, Matsuguchi T, et al. Dehydroepiandrosterone increased oxidative stress in a human cell line during differentiation. Free Radic Res 2009;43:922–31.
[35] Ho HY, Cheng ML, Chiu HY, Weng SF, Chiu DT. Dehydroepiandrosterone induces growth arrest of hepatoma cells via alteration of mitochondrial gene expression and function. Int J Oncol 2008;33:969–77.
[36] Barton RH. A decade of advances in metabonomics. Expert Opin Drug Metab Toxicol 2011;7:129–36.
[37] Lindon JC, Holmes E, Nicholson JK. So what's the deal with metabonomics? Anal Chem 2003;75:384A–91A.
[38] Wilson ID, Plumb R, Granger J, Major H, Williams R, Lenz EM. HPLC-MS-based methods for the study of metabonomics. J Chromatogr B 2005;817:67–76.
[39] Yang J, Xu G, Zheng Y, Kong H, Wang C, Zhao X, et al. Strategy for metabonomics research based on high-performance liquid chromatography and liquid chromatography coupled with tandem mass spectrometry. J Chromatogr A 2005;1084:214–21.
[40] Griffin JL, Nicholls AW. Metabolomics as a functional genomic tool for understanding lipid dysfunction in diabetes, obesity and related disorders. Pharmacogenomics 2006;7:1095–107.
[41] Nicholson JK, Lindon JC, Holmes E. 'Metabonomics': understanding the metabolic responses of living systems to pathophysiological stimuli via multivariate statistical analysis of biological NMR spectroscopic data. Xenobiotica 1999;29:1181–9.
[42] Fiehn O. Metabolomics – the link between genotypes and phenotypes. Plant Mol Biol 2002;48:155–71.
[43] Fiehn O. Combining genomics, metabolome analysis, and biochemical modelling to understand metabolic networks. Comp Funct Genomics 2001;2:155–68.
[44] Serkova NJ, Glunde K. Metabolomics of cancer. Meth Mol Biol 2009;520:273–95.
[45] Kim K, Aronov P, Zakharkin SO, Anderson D, Perroud B, Thompson IM, et al. Urine metabolomics analysis for kidney cancer detection and biomarker discovery. Mol Cell Proteomics 2009;8:558–70.
[46] Pradat PF, Dib M. Biomarkers in amyotrophic lateral sclerosis: facts and future horizons. Mol Diagn Ther 2009;13:115–25.
[47] Saude EJ, Obiefuna IP, Somorjai RL, Ajamian F, Skappak C, Ahmad T, et al. Metabolomic biomarkers in a model of asthma exacerbation: urine nuclear magnetic resonance. Am J Respir Crit Care Med 2009;179:25–34.
[48] Xu EY, Schaefer WH, Xu Q. Metabolomics in pharmaceutical research and development: metabolites, mechanisms and pathways. Curr Opin Drug Discov Devel 2009;12:40–52.
[49] Lindon JC, Holmes E, Nicholson JK. Metabonomics: systems biology in pharmaceutical research and development. Curr Opin Mol Therapeut 2004;6:265–72.
[50] Ho HY, Cheng ML, Wang YH, Chiu DT. Flow cytometry for assessment of the efficacy of siRNA. Cytometry A 2006;69:1054–61.
[51] Gao LP, Cheng ML, Chou HJ, Yang YH, Ho HY, Chiu DT. Ineffective GSH regeneration enhances G6PD-knockdown Hep G2 cell sensitivity to diamide-induced oxidative damage. Free Radic Biol Med 2009;47:529–35.
[52] Folch J, Lees M, Sloane Stanley GH. A simple method for the isolation and purification of total lipides from animal tissues. J Biol Chem 1957;226:497–509.
[53] Kanehisa M, Goto S. KEGG: kyoto encyclopedia of genes and genomes. Nucleic Acids Res 2000;28:27–30.
[54] Kanehisa M, Goto S, Furumichi M, Tanabe M, Hirakawa M. KEGG for representation and analysis of molecular networks involving diseases and drugs. Nucleic Acids Res 2010;38:D355–60.
[55] Wishart DS, Knox C, Guo AC, Eisner R, Young N, Gautam B, et al. HMDB: a knowledgebase for the human metabolome. Nucleic Acids Res 2009;37:D603–10.
[56] Ho HY, Cheng ML, Weng SF, Leu YL, Chiu DT. Antiviral effect of epigallocatechin gallate on enterovirus 71. J Agric Food Chem 2009;57:6140–7.
[57] Ho HY, Cheng ML, Weng SF, Chang L, Yeh TT, Shih SR, et al. Glucose-6-phosphate dehydrogenase deficiency enhances enterovirus 71 infection. J Gen Virol 2008;89:2080–9.
[58] Newman HA, Gordesky SE, Hoppel C, Cooper C. The action of digitonin on rat liver mitochondria. Phospholipid content. Biochem J 1968;107:381–5.
[59] Daum G. Lipids of mitochondria. Biochim Biophys Acta 1985;822:1–42.
[60] Kent C. Eukaryotic phospholipid biosynthesis. Annu Rev Biochem 1995;64:315–43.
[61] Hirao T, Urata Y, Kageyama K, Ikezaki M, Kawakatsu M, Matsuse M, et al. Dehydroepiandrosterone augments sensitivity to gamma-ray irradiation in human H4 neuroglioma cells through down-regulation of Akt signaling. Free Radic Res 2008;42:957–65.
[62] Shinno H, Noda C, Tanaka K, Ichihara A. Induction of L-lysine-2-oxoglutarate reductase by glucagon and glucocorticoid in developing and adult rats: in vivo and in vitro studies. Biochim Biophys Acta 1980;633:310–6.
[63] Yang H, Li TW, Peng J, Mato JM, Lu SC. Insulin-like growth factor 1 activates methionine adenosyltransferase 2A transcription by multiple pathways in human colon cancer cells. Biochem J 2011. doi:10.1042/BJ20101754.
[64] Sun HZ, Yang TW, Zang WJ, Wu SF. Dehydroepiandrosterone-induced proliferation of prostatic epithelial cell is mediated by NFKB via PI3 K/AKT signaling pathway. J Endocrinol 2010;204:311–8.
[65] Dashtaki R, Whorton AR, Murphy TM, Chitano P, Reed W, Kennedy TP. Dehydroepiandrosterone and analogs inhibit DNA binding of AP-1 and airway smooth muscle proliferation. J Pharmacol Exp Ther 1998;285:876–83.
[66] Martinez-Chantar ML, Garcia-Trevijano ER, Latasa MU, Martin-Duce A, Fortes P, Caballeria J, et al. Methionine adenosyltransferase II beta subunit gene expression provides a proliferative advantage in human hepatoma. Gastroenterology 2003;124:940–8.
[67] Wang Q, Liu QY, Liu ZS, Qian Q, Sun Q, Pan DY. Lentivirus mediated shRNA interference targeting MAT2B induces growth-inhibition and apoptosis in hepatocelluar carcinoma. World J Gastroenterol 2008;14:4633–42.
[68] Kapyaho K, Poso H, Janne J. Role of propylamine transferases in hormone-induced stimulation of polyamine biosynthesis. Biochem J 1980;192:59–63.
[69] Ikeguchi Y, Bewley MC, Pegg AE. Aminopropyltransferases: function, structure and genetics. J Biochem 2006;139:1–9.
[70] Igarashi K, Kashiwagi K. Modulation of cellular function by polyamines. Int J Biochem Cell Biol 2010;42:39–51.
[71] Coburn RF. Polyamine effects on cell function: Possible central role of plasma membrane PI(4,5)P2. J Cell Physiol 2009;221:544–51.
[72] Ray RM, Zimmerman BJ, McCormack SA, Patel TB, Johnson LR. Polyamine depletion arrests cell cycle and induces inhibitors p21(Waf1/Cip1), p27(Kip1), and p53 in IEC-6 cells. Am J Physiol 1999;276:C684–91.
[73] Choi SH, Kim SW, Choi DH, Min BH, Chun BG. Polyamine-depletion induces p27Kip1 and enhances dexamethasone-induced G1 arrest and apoptosis in human T lymphoblastic leukemia cells. Leuk Res 2000;24:119–27.

[74] Vaz FM, Wanders RJ. Carnitine biosynthesis in mammals. Biochem J 2002;361: 417–29.
[75] Noland RC, Koves TR, Seiler SE, Lum H, Lust RM, Ilkayeva O, et al. Carnitine insufficiency caused by aging and overnutrition compromises mitochondrial performance and metabolic control. J Biol Chem 2009;284:22840–52.
[76] Zeisel SH, Blusztajn JK. Choline and human nutrition. Annu Rev Nutr 1994;14:269–96.
[77] Sharpley MS, Shannon RJ, Draghi F, Hirst J. Interactions between phospholipids and NADH:ubiquinone oxidoreductase (complex I) from bovine mitochondria. Biochemistry 2006;45:241–8.
[78] Baykal AT, Jain MR, Li H. Aberrant regulation of choline metabolism by mitochondrial electron transport system inhibition in neuroblastoma cells. Metabolomics 2008;4:347–56.
[79] Hoch FL. Cardiolipins and biomembrane function. Biochim Biophys Acta 1992;1113:71–133.
[80] Schlame M, Otten D. Analysis of cardiolipin molecular species by high-performance liquid chromatography of its derivative 1,3-bisphosphatidyl-2-benzoyl-sn-glycerol dimethyl ester. Anal Biochem 1991;195:290–5.
[81] Schlame M, Ren M, Xu Y, Greenberg ML, Haller I. Molecular symmetry in mitochondrial cardiolipins. Chem Phys Lipids 2005;138:38–49.
[82] Mileykovskaya E, Zhang M, Dowhan W. Cardiolipin in energy transducing membranes. Biochemistry (Mosc) 2005;70:154–8.
[83] Lange C, Nett JH, Trumpower BL, Hunte C. Specific roles of protein-phospholipid interactions in the yeast cytochrome bc1 complex structure. Embo J 2001;20:6591–600.
[84] Tuominen EK, Wallace CJ, Kinnunen PK. Phospholipid-cytochrome c interaction: evidence for the extended lipid anchorage. J Biol Chem 2002;277: 8822–6.
[85] Schlame M, Rua D, Greenberg ML. The biosynthesis and functional role of cardiolipin. Prog Lipid Res 2000;39:257–88.
[86] Zhang M, Mileykovskaya E, Dowhan W. Gluing the respiratory chain together. Cardiolipin is required for supercomplex formation in the inner mitochondrial membrane. J Biol Chem 2002;277:43553–6.
[87] Mileykovskaya E, Dowhan W. Cardiolipin membrane domains in prokaryotes and eukaryotes. Biochim Biophys Acta 2009;1788:2084–91.
[88] Xu Y, Malhotra A, Ren M, Schlame M. The enzymatic function of tafazzin. J Biol Chem 2006;281:39217–24.
[89] Claypool SM, Boontheung P, McCaffery JM, Loo JA, Koehler CM. The cardiolipin transacylase, tafazzin, associates with two distinct respiratory components providing insight into Barth syndrome. Mol Biol Cell 2008;19:5143–55.
[90] Panayiotidis MI, Stabler SP, Allen RH, Pappa A, White CW. Oxidative stress-induced regulation of the methionine metabolic pathway in human lung epithelial-like (A549) cells. Mutat Res 2009;674:23–30.
[91] Hitchler MJ, Domann FE. An epigenetic perspective on the free radical theory of development. Free Radic Biol Med 2007;43:1023–36.
[92] Wiswedel I, Gardemann A, Storch A, Peter D, Schild L. Degradation of phospholipids by oxidative stress–exceptional significance of cardiolipin. Free Radic Res 2010;44:135–45.
[93] Kim J, Minkler PE, Salomon RG, Anderson VE, Hoppel CL. Cardiolipin: characterization of distinct oxidized molecular species. J Lipid Res 2011;52:125–35.